Enhanced edge Thomson scattering on MAST

R. Scannell, M. J. Walsh, P. G. Carolan, N. J. Conway, A. C. Darke, M. R. Dunstan, D. Hare, and S. L. Prunty

Citation: Review of Scientific Instruments **77**, 10E510 (2006); doi: 10.1063/1.2237488
View online: https://doi.org/10.1063/1.2237488
View Table of Contents: http://aip.scitation.org/toc/rsi/77/10
Published by the American Institute of Physics

Enhanced edge Thomson scattering on MAST

R. Scannell[a)]
EURATOM/UKAEA Fusion Association, Culham Science Centre, Abingdon, Oxon OX14 3DB, United Kingdom and Department of Electrical and Electronic Engineering, University College Cork, Association EURATOM-DCU Ireland

M. J. Walsh, P. G. Carolan, N. J. Conway, A. C. Darke, M. R. Dunstan, and D. Hare
EURATOM/UKAEA Fusion Association, Culham Science Centre, Abingdon, Oxon OX14 3DB, United Kingdom

S. L. Prunty
Department of Electrical and Electronic Engineering, University College Cork, Association EURATOM-DCU, Ireland

(Received 9 May 2006; presented on 8 May 2006; accepted 3 July 2006; published online 3 October 2006)

A new edge Thomson scattering diagnostic has been implemented at MAST to complement an existing high spatial resolution ruby laser system and the high time sampling core Nd:YAG system. The Nd:YAG system comprises of four independently controllable lasers. Scattered light from these lasers is viewed at large scattering angle (153°) by a special optical arrangement in the new edge system. The Nd:YAG lasers are viewed at 16 contiguous spatial locations separated by ~1 cm each, located at the plasma outboard pedestal and scrape-off layer region. Here the use of a low f-number lens for the collection of a large solid angle of scattered light is particularly beneficial due to low plasma density (n_e). The spectrum of scattered light is significantly broader at large scattering angles, allowing diagnosis of lower plasma temperatures (T_e) while using the same spectrometer design as the core system. The four Nd:YAG lasers follow two separate slightly offset ($<1/3$ of a spatial channel) optical paths through the vessel. This is useful when the lasers are used in burst mode for detailed edge studies of fast events such as ELMs. Polychromators have been designed to allow for both Raman and Rayleigh calibration. First results from this diagnostic are presented showing H-mode pedestal behavior. A novel spectral fitting technique has been devised and is applied to edge pedestal fitting. © *2006 American Institute of Physics.* [DOI: 10.1063/1.2237488]

I. INTRODUCTION

The edge system enhancement is designed to meet the physics needs of high spatial resolution with low error at the plasma outboard edge. Current physics programs are particularly interested in resolving the outboard temperature pedestal and in the behavior of the plasma edge during ELMs. The new threshold shift (TS) diagnostic views the existing Nd:YAG (yttrium aluminum garnet) lasers using viewing optics in the same port as the laser with a scattering angle of 150°–156°. The two existing TS diagnostics view the Nd:YAG and ruby lasers using optics approximately orthogonal to the lasers' path through the vessel. The views of both the core and edge TS Nd:YAG systems of the laser path through the vessel are illustrated in Fig. 1. The existing Nd:YAG system is described in Ref. 1 and has 19 spatial points across the edge and core of the plasma. The time resolution of both Nd:YAG systems is 200 Hz, obtained from the combination of four 50 Hz 1 J lasers. The ruby laser system obtains a 300 point spatial profile once per plasma shot and is described in Ref. 2.

[a)]Electronic mail: rory.scannell@ukaea.org.uk

II. SYSTEM DESIGN

The edge system optics focus on the laser from 1.20 to 1.50 m along the plasma major radius. Currently 16 spatial channels from 1.29–1.45 m are populated, capturing approximately one-third of a plasma minor radius on a typical MAST shot. Scattering lengths of 10–12 mm are used which are significantly less than the 26–40 mm in the core system. The extra photon count necessary to compensate for decrease in scattering volume is achieved by the proximity of the collection optics to the laser beam (an $f/6$ lens is used). The composite lens is made up of four individual lenses, held in a tubular collection cell of 5 mm thick aluminium indicated as *edge collection optics* in Fig. 1. This lightweight system design (~25 kg) allows the collection cell to be bolted to the machine. A stainless steel spacer is placed between the machine and the collection cell to provide the thermal insulation of optical components during vacuum vessel baking. The laser beam is imaged telecentrically, so optical fiber bundles can be held parallel. The fiber bundle support structure allows for vertical and rotatable adjustment to optimize the laser view. These are adjusted for optimal viewing of all four lasers during a Raman scattering.

Wiregrid polarizers have been built into the lens design and allow for the high rejection of that component of back-

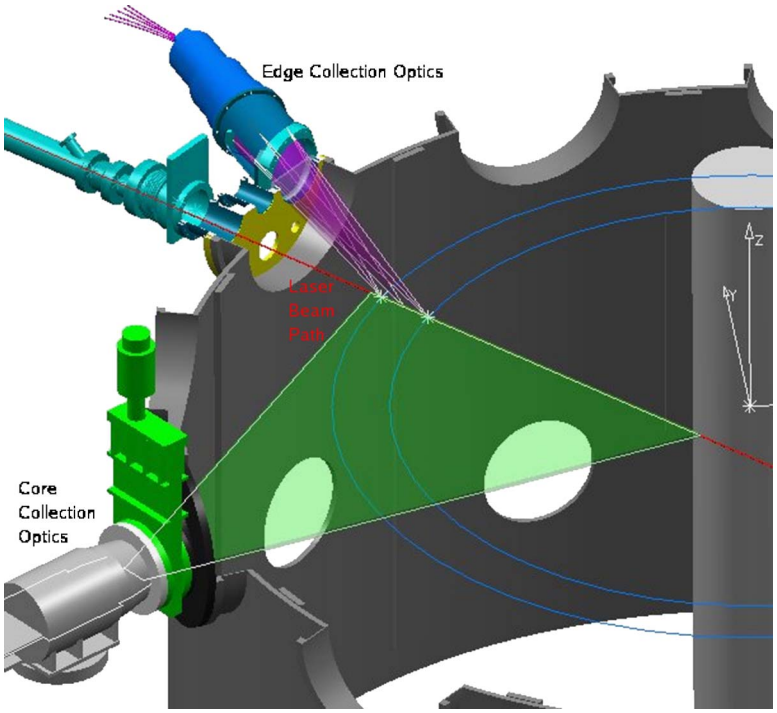

FIG. 1. (Color online) Layout of the MAST vacuum vessel, showing views of edge and core optics of the Thomson scattering laser. The major radii viewed are schematically illustrated, the core system viewing from ~0.4–1.5 m, edge system viewing from 1.25–1.45 m indicated by blue lines. The edge system collection optics use the same port as the laser.

ground plasma light with polarization perpendicular to the scattered light.[3] These polarizers are broadband and have good transmission of the desired polarization. The polarization of Raman scattered light is considered in absolute calibration, since it has components both parallel and perpendicular to scattered light.

Scattered light is transmitted from the vessel to polychromators in the TS laboratory using fiber optics. Each polychromator is optically duplexed, so that it receives two scattered signals originating from two spatial points transmitted by different lengths of optical fibres. The different lengths provide different optical delays, so scattered signals from different spatial points can be discriminated by their arrival times.

Polychromators have five interference filters, four of which measure Thomson scattered light. The fifth filter is a high-pass filter transmissive at the laser wavelength to allow for the possibility of absolute calibration using Rayleigh scattering. During Rayleigh scattering Wratten filters are used to reduce scattered light levels. Two of the interference filters allow for Raman calibration, having central wavelengths of 1047.3 and 1057.7 nm and bandwidths of 14.3 and 5.5 nm, respectively. At room temperature Raman scattering off N_2 gas produces similar cross sections for both of these channels. The comparison of an absolute calibration using both of these channels reduces the possibility of bias being introduced to the Raman calibration. The proximity of these channels to the laser wavelength, 1064.4 nm, allows for the measurement of low electron temperatures. Scattered signals are measured using 1 GHz analog-to-digital converters (ADCs) and have durations comparable with the laser pulse duration of the order of 10 ns. The low frequency light in the signals due to background light is measured separately using slow sampling 100 kHz ADCs. Low frequency background light level is negligible for narrow spectral channels but comparable to the scattered signal levels for broad spectral channels.

The system parameters used to determine the achievable fractional errors that can be measured by the system are shown in Fig. 2. The signal error estimate on each channel is derived from the amount of background and scattered light measured, as well as a small component due to amplifier noise. Figure 2 shows that temperatures as low as a few eV and up to a few thousand eV can be measured. Should higher temperature coverage be required, extra spectral channels may be added, as the polychromators are designed to hold up to seven interference filters.

III. ANGULAR CONSIDERATIONS

The étendue for background light is constant as a function of scattering angle. The scattering volume, however, increases as a function of scattering angle as the optics view

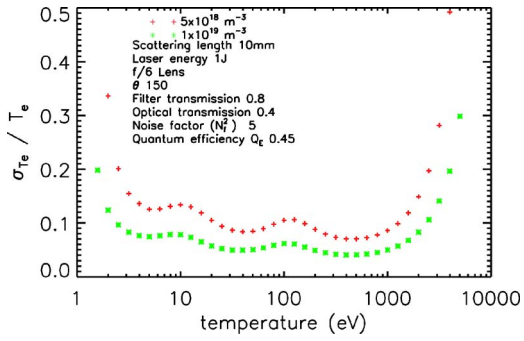

FIG. 2. (Color online) Fractional temperature error as a function of T_e for an edge system spectrometer as calculated from photon accounting methods. Q_E is calculated at the peak transmission of that wavelength channel closest to the laser wavelength.

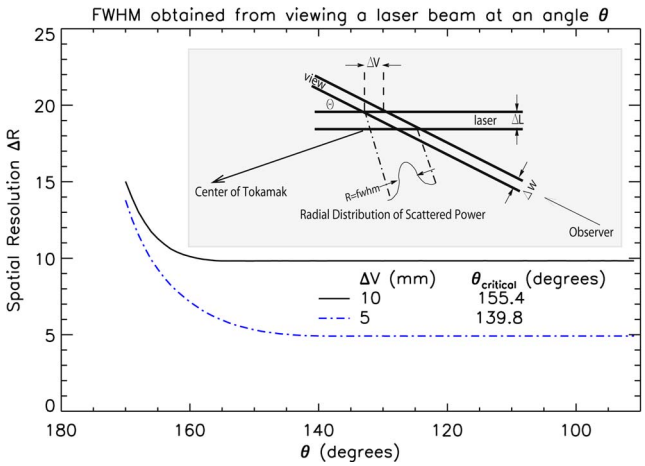

FIG. 3. (Color online) Effect of high angle scattering on acchieved radial resolution.

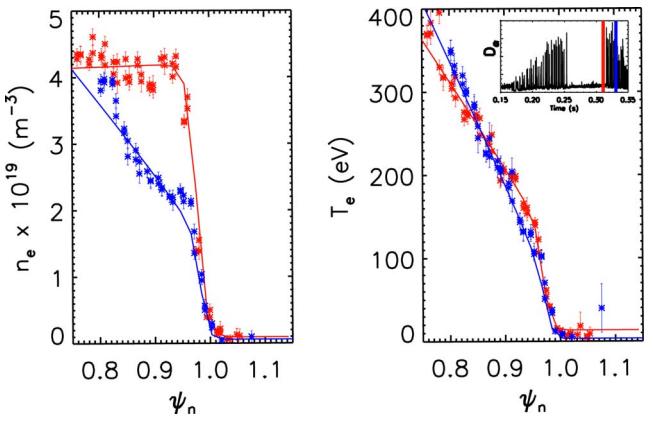

FIG. 4. (Color online) Convective nature of ELMs on MAST. Inset figure shows the timing of the measured profiles from a divertor D_α trace. Profiles are obtained 20 ms apart, during ELM-free *H*-mode and during ELM-ing *H*-mode. Significant particle loss can be seen, although the temperature pedestal is similar for both times. The profiles are fitted using the spectral fitting technique described.

along the laser beam increases. A simple geometric analysis shows that the ratio of scattered light to background plasma light scales as $1/\sin\theta$, where θ is the scattering angle (see Fig. 2). Hence scattering at 150° gives a signal to background plasma light ratio of twice that of 90° scattering.

The four Nd:YAG lasers follow two different laser paths through the vessel as described in Ref. 1. The two beam paths overlap close to the center of the vessel but are separated by a few millimeters at the vessel entrance. This makes little difference to the radial positions of the scattering volumes as seen by the core Nd:YAG system. However, since the edge system views short radial scattering lengths (relative to the laser width) at high angle, this offset means that slightly different radial positions are observed by the same collection fiber for the two beam paths. This allows spatial resolution of better than one scattering length, when lasers are fired over short time intervals.

Low T_e measurements are often limited by the width of the wavelength distribution of the scattered spectrum. Lower T_e is easier to measure at large scattering angle, since the scattered spectrum is broader for the same T_e, scaling as $\Delta\lambda \propto \sin(\theta/2)$. Hence at large scattering angle, for a given plasma density, the minimum T_e which produces a measurable signal in the two spectral channels closest to the laser wavelength will be decreased.

Large angle scattering can degrade the spatial resolution achieved. For the purposes of this discussion, the achieved radial resolution (Δ_r) is defined as the full width at half maximum (FWHM) of the radial distribution of scattered power for each scattering volume and the view width (ΔV) is defined as the length of optical view parallel to the laser beam. These are illustrated in Fig. 3. The minimum spatial resolution achievable becomes limited by the laser width (ΔL) at high angle. Laser width for these calculations is taken as 5 mm, which contains 90% of the power of the MAST Nd:YAG laser at the edge system radii. Figure 3 shows the radial resolution achieved for view widths of 10 and 5 mm. At 90°, arbitrarily small resolution may be obtained equal to the view width. For diagnostic views at steeper angles to the laser, the scattered light originates from a broader radial extent. The rate of increase of achieved radial resolution becomes large after a critical angle θ_{critical} is exceeded. Physically, θ_{critical} may be understood as the minimum angle where the laser view encompasses a horizontal cross section of the laser orthogonal to the laser direction. Beyond this any increase in scattering angle leads to a large increase in radial distribution of scattered power. The MAST edge TS system view widths are ~10 mm, and hence from Fig. 3, the spatial resolution achieved approximates to the view width. Calculations have been adjusted for MAST geometry, which includes an angular offset for a nonradial laser beam path (see Fig. 1).

IV. RESULTS

The measurement of the outboard pedestal is one of the primary design objectives of this system. Figure 4 shows data obtained from the edge system during a MAST *H*-mode shot. The four Nd:YAG lasers were fired in burst mode 5 μs apart to produce two sets of profiles at two time points. The first, indicated by the red points, is taken during ELM-free *H*-mode. The second indicated by the blue points, is taken during ELM-ing *H*-mode in the inter-ELM period. It is observed that the n_e pedestal falls significantly upon transition to ELM-ing *H*-mode, while the T_e pedestal is apparently unaffected by the transition. These convective ELMs are typical of MAST ELMs and have been observed on MAST using the ruby TS diagnostic[5] and termed "minimum" by Ref. 4 when observed in JET. A novel technique used to fit these pedestal profiles is discussed in detail in the next section.

Figure 5 shows a result obtained from the edge system during an ELM. The four lasers are fired 5 μs apart to capture the evolution of a single ELM filament. The timing of the lasers relative to the divertor D_α emission is shown on the inset figure. The blue curve shows a typical *H*-mode edge profile; the red trace shows the edge n_e profile then push out with no change to the pedestal top n_e. The green profile shows a large density "hole" inside the pre-ELM last closed flux surface (LCFS) and a separated structure that is considered to be filamentary in nature. The final orange profile shows this filament pushed further out. Considering the ve-

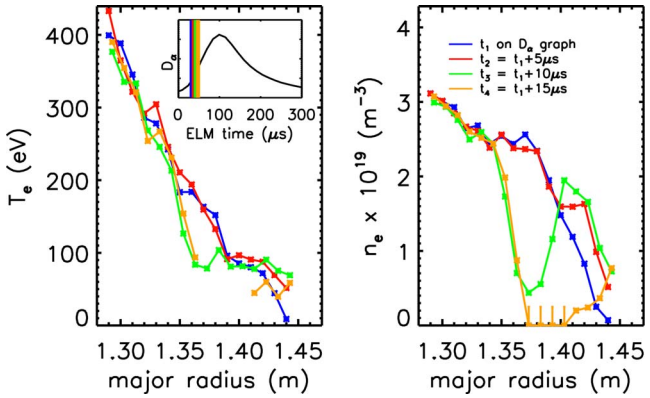

FIG. 5. (Color online) Filament observed during an ELM event using the lasers in burst mode fired 5 μs apart.

locity to be purely radial, the 8 cm movement in 5 μs corresponds to a radial velocity of $\sim$16 km s^{-1}. A number of filamentary structures have been observed during ELMs using the edge TS diagnostic; these are discussed in detail in Ref. 6.

V. INTEGRATED SPECTRAL FITTING

A technique of spectral fitting is used to fit the profiles obtained. This incorporates simultaneously T_e and n_e pedestal profiles in deriving composite spectra that are fitted to the measured spectral data. This technique has a number of advantages over conventional fitting techniques. Covariance between T_e and n_e ($\sigma_{n_e T_e}$) obtained when performing a fit to a single point is discarded if T_e and n_e radial profiles are then separately fitted, since only parameter error (σ_{T_e} and σ_{n_e}) is used. Spectral fitting makes use of this covariance term. In the case of Fig. 4 both the edge T_e and n_e profiles are assumed to have modified tanh functional forms; however, the spectral fitting technique works for any general form. Here modified tanh function parameters describing both the T_e and n_e pedestals are used to generate spectra to best fit measured spectral data.

In a region of T_e and n_e gradients, the measured T_e profile is weighted by the intensity function n_e. Hence, deconvolution of the T_e pedestal is best performed by fitting spectra described by n_e and T_e pedestal parameters convolved by the radial instrument function to the measured spectra rather than fitting a radial profile of T_e convolved by the radial instrument function to the measured T_e profile. The convolution of the radial profile of T_e without inclusion of the intensity weighting by n_e introduces systematic errors in the calculation of pedestal parameters. These biases are particularly acute when the scattering length is large compared to the temperature scale lengths or pedestal width (Δ_{T_e}). The systematic error in the n_e pedestal fit will be smaller, since the n_e profile and instrument functions are both intensity functions.

An oversampled system, in which the distance between adjacent spatial samples is less than the scattering length, will produce the largest biases in Δ_{T_e} and the position of the temperature pedestal knee if Δ_{T_e} is not much greater than scattering length. The edge system is oversampled, when lasers are fired in burst mode microseconds apart to obtain better pedestal resolution. As discussed already, different radial positions for scattering centers are observed by the same viewing fiber for lasers following slightly offset paths. This allows us to obtain spatial resolution of up to $\Delta_r/2$, while the radial instrument function FWHM as already discussed approximates to Δ_r.

Results from simulations performed have shown that for a system with $\Delta_{n_e}=\Delta_r=\Delta_{T_e}=10$ mm, using conventional deconvolution, the temperature pedestal position measurement is biased $\sim$2 mm outside of its actual position and there are significant disadvantages to recovery of Δ_{T_e}. Spectral fitting removes these biases. Simulations for the case $\Delta_{n_e}=\Delta_{T_e}=5$ mm and $\Delta_r=10$ mm, where profiles are spatially sampled at 5 mm resolution, show that conventional fitting produces a mean error of 3.6 mm for Δ_{T_e} and 1.74 mm for Δ_{n_e} while spectral fitting produces mean errors of 1.85 mm for Δ_{T_e} and 1.26 mm for Δ_{n_e}.

VI. SYSTEM PERFORMANCE

Raman calibration can be used to relate scattered signal variance to scattered signal magnitude. This determines the Poisson error on the system including nonidealities and can then be used to determine achieved fractional temperature error $\sigma_{T_e,\text{achieved}}/T_e$. Comparison of this value with the theoretical value from photon accounting estimates $\sigma_{T_e,\text{ideal}}/T_e$ gives a measure of system performance (η). Fractional temperature errors can be shown to relate directly to fractional signal errors for a large signal.

$$\eta = \frac{\sigma_{T_e,\text{ideal}}}{\sigma_{T_e,\text{achieved}}}.$$

The performance of the spectrometers in the edge system by this measure are in the range of $\eta = 80\% - 90\%$. This measure of performance is not directly related to an optical throughput efficiency because actual noise factor may be different to the theoretical noise factor and also Raman calibration sees the nonidealities of signal measurement, such as ADC noise and amplifier noise.

ACKNOWLEDGMENTS

This work was supported by the Engineering and Physical Sciences Research Council and by the European Communities under the contract of Association between EURATOM and UKAEA. The views and opinions expressed herein do not necessarily reflect those of the European Commission. The authors are indebted to R. Huxford for his contributions.

[1] M. J. Walsh *et al.*, Rev. Sci. Instrum. **74**, 1663 (2003).
[2] M. J. Walsh *et al.*, Rev. Sci. Instrum. **70**, 742 (1999).
[3] M. J. Walsh *et al.*, Rev. Sci. Instrum. **75**, 3909 (2004).
[4] A. Loarte, *et al.*, Plasma Phys. Controlled Fusion **44**, 14815 (2002).
[5] A. Kirk *et al.*, Plasma Phys. Controlled Fusion **46**, A187 (2004).
[6] R. Scannell *et al.*, Proceedings of the 33rd EPS Conference on Plasma Physics, 2006 (unpublished).